AIAA JOURNAL
Vol. 34, No. 4, April 1996

Systematic Study of the Correlation Between Geometrical Disturbances and Flow Asymmetries

Yuval Levy* and Lambertus Hesselink†
Stanford University, Stanford, California 94305-4035
and
David Degani‡
Technion—Israel Institute of Technology, Haifa 32000, Israel

Recently, large efforts were directed to numerical simulations of high-incidence flows around slender bodies of revolution to gain more insight into the problem of flow asymmetry. One of the significant advantages in using numerical simulation to investigate these flows is the ability to obtain a disturbance-free base solution. This base solution can then be perturbed for parametric studies of controlled disturbances. The experimentally observed asymmetric flow is numerically simulated by the introduction of a simulated disturbance (bump) placed near the body apex. A series of asymmetric flows over an ogive cylinder at a high angle of attack is computed by systematically varying the bump size. The results reproduce the experimentally observed effect of nose imperfections on flow asymmetry and are used to demonstrate the role of the sectional side force variation along the body. Analysis of the numerical results and the correlation between the disturbances and the asymmetric flow point to a convective instability mechanism as the origin of flow asymmetry.

Introduction

WHEN a slender body of revolution is placed at a high angle of attack (typically an angle between 30 and 50 deg), the flow around it becomes asymmetric, and the body experiences a side force and a yawing moment.[1–3] The flow asymmetry is characterized by asymmetric pairs of vortices that curve away from the body from alternate sides and ultimately virtually align themselves with the freestream direction. The flow in this regime is highly sensitive to small disturbances, including infinitesimal surface roughness around the nose as well as disturbances originating in the freestream. Experimental results also show that the asymmetry is highly dependent on the roll angle of the model relative to the oncoming flow.[1,4–8]

The phenomenon of asymmetric flow around slender bodies of revolution at high incidence has been known to exist since the early 1950s. It was first brought to light in two reports by Allen and Perkins.[9,10] Analysis of the flow-visualization experiments that they conducted led them to propose a model for the flow. According to the model, which has come to be known as the impulsive flow analogy, the development of the crossflow with distance along the body behaves in a similar way to the development with time of the flow around a two-dimensional circular cylinder after it is impulsively started from rest. On that basis, Allen and Perkins were led to postulate the existence of a stationary asymmetric flow around long inclined bodies of revolution. Thomson and Morrison[11] were able to interpret schlieren photographs of high-angle-of-attack flows by an application of the model. The vortical structure that emerged from use of the model was consistent with the photographs, i.e., vortices that curve away from the body from alternate sides and move downstream at a small angle to the freestream direction.

Later results from investigations of flows around ogive-cylinder bodies conducted by Hunt and Dexter[4] and Dexter and Hunt[5] revealed that the pattern of vortices that detach from the body and curve away from alternate sides results in a lengthwise-periodic distribution of the sectional side force that similarly alternates in sign. By conducting simultaneous flow visualization and force measurements they were able to show that the sectional side force is directed toward the side containing the vortex that lies closer to the body (because of the larger suction that it generates). The sectional normal-force distribution along the body is also lengthwise periodic but is single signed and has smaller amplitudes and a higher frequency.

The first successful numerical simulation of fully three-dimensional asymmetric flows was achieved by Degani[12,13] and Degani and Schiff.[14] Their study, aimed at revealing the origin of flow asymmetry, pointed to the necessity of maintaining a fixed asymmetric disturbance to sustain the flow asymmetry. Based on the observation that removal of the disturbance allowed the flow to return to the undisturbed symmetric state, Degani[12,13] suggested that there is a flow regime (roughly between $\alpha = 30$ and 50 deg) where the asymmetry is the result of a convective instability mechanism. (Numerical simulations obtained on the basis of a conical flow assumption[15,16] show that asymmetric conical solutions can be obtained without fixed perturbations. These results are consistent with the presence of an absolute instability mechanism. The authors believe that the conical assumption, by eliminating one coordinate direction, eliminates the possibility of convective instability mechanism coming into play and forces the occurrence of the absolute instability mechanism.)

The results of the numerical simulations presented by Degani[12,13] were the initial motivation for an extensive experimental investigation that was conducted by Zilliac et al.[8] Side force variations with role angle position were measured at angles of attack ranging from $\alpha = 20$ to 90 deg. The experimental results showed that as the angle of attack is changed between $30 \leq \alpha \leq 50$ deg, the side force response to roll angle position changes from a continuous periodic function (with growing amplitudes) to an almost discontinuous square-wave variation, known as a bistable variation. Another interesting revelation made by Zilliac et al. was the effect of dust particles on the side force variation. They found that the trends of the side force response to roll angle position could change over time. Dust particles that had coated the nose caused a change that was overturned by cleaning the nose. This was another indication of how sensitive these flows are to nose imperfections.

Experimental studies conducted by Degani and Tobak[17,18] and Williams and Bernhardt[19] suggest that the stationary asymmetric

Presented as Paper 95-0365 at the AIAA 33rd Aerospace Sciences Meeting, Reno, NV, Jan. 10–12, 1995; received Jan. 30, 1995; revision received Aug. 2, 1995; accepted for publication Nov. 27, 1995.

*Postdoctoral Fellow, Aeronautics and Astronautics Department. Member AIAA.
†Professor, Electrical Engineering and Aeronautics and Astronautics Departments. Member AIAA.
‡Professor, Faculty of Mechanical Engineering. Associate Fellow AIAA.

flows are a result of a convective instability mechanism in this regime of the flow. They have shown experimentally that a small symmetry-breaking disturbance, acting on the body's surface near the tip, is sufficient to excite an asymmetric flow component that vanishes when the disturbance is removed. In a more recent experiment, Degani and Tobak[20] reproduced this type of behavior by disturbing the flow upstream of the body, providing additional evidence of the existence of a convective instability mechanism.

In a computational study paralleling the experimental effort,[17,18,20] Degani and Levy[21] used a time-marching thin-layer Navier–Stokes code and a simulated disturbance (a bump) placed near the body apex in an attempt to numerically simulate the particular asymmetric turbulent flows experimentally observed by Lamont.[6] After a systematic variation of the bump height revealed the one most representative of the net effect of nose roughness for each of the roll angle orientation in Lamont's experiment,[6] it was found possible to achieve a quantitative agreement between the numerical and experimental results.

The favorable comparisons reported in Ref. 21 suggested that it might be possible to systematically study the effect of disturbance height on the resulting asymmetric flow. Such a study is the subject of this paper. Computations are carried out about a 3.5 caliber tangent ogive-cylinder body with an overall length-to-diameter ratio of 7.5. A model having this geometry was extensively tested by Lamont[6] in the NASA Ames Research Center 12-ft pressure wind tunnel, and detailed surface pressure distributions were obtained at Reynolds numbers ranging from $Re_D = 2.0 \times 10^5$ to 4.0×10^6 and angles of attack ranging from $\alpha = 20$ to 90 deg. The time-marching thin-layer Navier–Stokes code is utilized to compute a series of subsonic turbulent flows over an ogive cylinder for the flow conditions: $M_\infty = 0.28$, angle of attack $\alpha = 40$ deg, and Reynolds number $Re_D = 3.0 \times 10^6$. Each numerical solution of the series corresponds to a different bump height. The series of solutions provides the means to systematically study the effect of nose imperfections on asymmetric flows. A well-defined progression of the flow asymmetry as a function of the bump height is demonstrated. The quantitative and qualitative agreements between the computational and experimental results show that the wide variety of physical phenomena observed in the experiments could be captured by using a suitable algorithm and a single disturbance. Results confirm the correlation between the vortical structure and the variation of sectional side force coefficient along the body that was observed by Hunt and Dexter[4] and Dexter and Hunt.[5]

Theoretical Background

The equations governing fluid flow are derived from the laws of conservation of mass, momentum, and energy. The set of five partial differential equations is known as the Navier–Stokes equations and can be represented in a conservation law form that is convenient for numerical simulations. Written in body-fitting curvilinear coordinates, these equations take the form

$$\partial_\tau \hat{Q} + \partial_\xi (\hat{E} - \hat{E}_v) + \partial_\eta (\hat{F} - \hat{F}_v) + \partial_\zeta (\hat{G} - \hat{G}_v) = 0 \quad (1)$$

where τ is the time, and the independent spatial variables ξ, η, and ζ are the streamwise, circumferential, and radial coordinates, respectively. In Eq. (1) $\hat{Q}$ is the vector of dependent flow variables, mass, momentum, and energy; $\hat{E} = \hat{E}(\hat{Q})$, $\hat{F} = \hat{F}(\hat{Q})$, and $\hat{G} = \hat{G}(\hat{Q})$ are the inviscid flux vectors; whereas the terms $\hat{E}_v$, $\hat{F}_v$, and $\hat{G}_v$ are fluxes containing the viscous derivatives.

For body-conforming coordinates and flow at high Reynolds number (with ζ the coordinate leading away from the surface), the thin-layer approximation can be applied. By using nondimensional variables, the Reynolds number Re can be factored out and Eq. (1) takes the following form[22,23]:

$$\partial_\tau \hat{Q} + \partial_\xi \hat{E} + \partial_\eta \hat{F} + \partial_\zeta \hat{G} = Re^{-1} \partial_\zeta \hat{S} \quad (2)$$

The equation of state is used to compute the pressure from the known flow variables.

The implicit scheme employed in this study is the algorithm reported by Steger et al.[24] The two-factor implicit algorithm is obtained by using upwind differencing of the convective terms in the streamwise direction and central differencing in the radial and circumferential directions. It has been shown that this algorithm is unconditionally stable for a representative model wave equation.[25]

The computational mesh consists of 120 equispaced circumferential planes extending completely around the body. In each circumferential plane the mesh contains 50 radial points between the body surface and the computational outer boundary and 59 axial points between the nose and the rear of the body. The computed body length is extended 3.0 cylindrical diameters beyond the physical length of the body, to a total of 10.5 diameters, to minimize the effect of the outflow boundary conditions. The nondimensional cylinder diameter is $D = 1.0$, and the minimum grid spacing at the body surface is chosen to be $\Delta\zeta = 0.00001$ to maintain a value of $y^+ < 5$ at the first shell of points above the surface. Together with proper radial stretching, this ensures having at least 20 grid points within the viscous layer. The outer boundary is located 11 body diameters from the body surface.

The boundary conditions applied in the present computations were chosen to simulate viscous flows. The wall boundary conditions enforce zero slip and adiabatic wall conditions. The contravariant velocities are set to zero, and a zeroth-order normal pressure gradient condition is applied. The inflow boundary condition enforces freestream conditions, whereas the exit boundary condition is a simple zeroth-order zero-axial-gradient extrapolation condition. A periodic boundary condition is applied, allowing the flow to become asymmetric, if warranted by the flow physics.

An algebraic turbulence model is utilized to calculate the coefficients of viscosity and thermal conductivity. It was developed originally by Baldwin and Lomax[22] for a flat-plate boundary layer, based on the two-layer model reported by Cebeci et al.,[26] and was later modified by Degani and Schiff[27] to be applicable to flowfields containing crossflow separation. The modified model has been used successfully to simulate subsonic as well as supersonic symmetric flows[27,28] and was also successfully applied in numerical simulations of asymmetric flows.[21]

Examination of Previous Results

In previous work, Degani and Levy[21] presented results from numerical simulations of subsonic turbulent flows over an ogive cylinder for the following flow conditions: $M_\infty = 0.2$, angle of attack $\alpha = 30$ deg, and Reynolds numbers $Re_D = 3.0 \times 10^6$ and 4.0×10^6 (each utilizing a different bump height to simulate the asymmetry level of the experimental results); and $M_\infty = 0.28$, angle of attack $\alpha = 40$ deg, and Reynolds number $Re_D = 3.0 \times 10^6$ for one bump height. Results for all three cases were compared against results from Lamont's experiment[6] and a good agreement was demonstrated. However, the behavior of the sectional side force coefficient along the body was not presented. In the following sections it will be shown that this behavior can be reproduced by numerical simulations, again by the choice of an appropriate bump height.

Ogive Cylinder Flow at $\alpha = 30$ deg

The experimental results for the flow at the angle of attack $\alpha = 30$ deg and Mach number $M_\infty = 0.2$ included pressure measurements for Reynolds numbers ranging from $Re_D = 2.0 \times 10^5$ to 4.0×10^6 but included only one roll angle orientation per Reynolds number. The two cases that were chosen for the simulation—$Re_D = 3.0 \times 10^6$ and roll angle $\phi = 0.8$ deg, and $Re_D = 4.0 \times 10^6$ and roll angle $\phi = 89.6$ deg—exhibited a small and a large asymmetry, respectively. As a result of the different roll angles, each of these cases had a different set of surface roughness disturbances that were numerically simulated by the appropriate bump size. The geometry of the bump is illustrated by a top view of the body apex in Fig. 1. Note that the portion of the body presented in the figure is only 1% of the total body length. The shape, axial location, and circumferential location ($\phi = 90$ deg) of the bump were fixed for all cases considered in this work. The height of the bump (h) was the only parameter that was varied. In Fig. 1 the bump height is $h = 0.01D$ or approximately 25% of the local diameter. Results for the case of a small asymmetry were obtained with the use of a small bump ($h/D = 0.0025$), whereas results for the large asymmetry case were obtained with the use of a larger bump ($h/D = 0.01$).

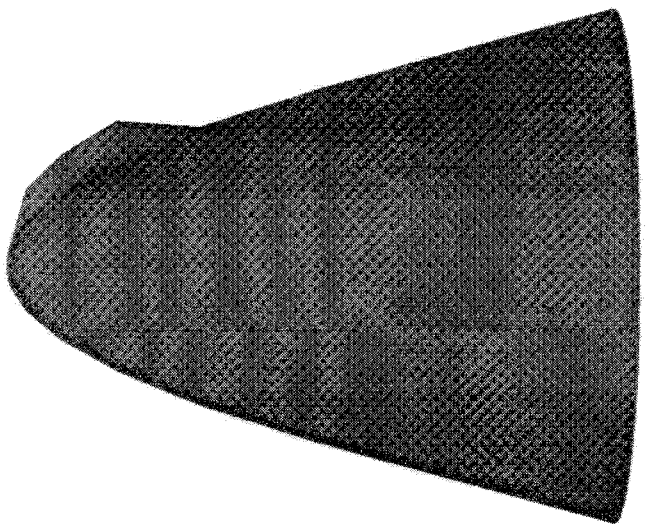

Fig. 1 Plan view of nose tip with geometrical disturbance ($h/D = 0.01$).

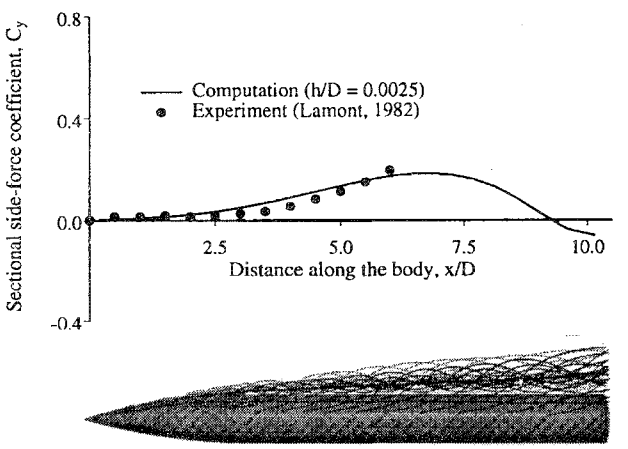

Fig. 2 Computed off-surface streamlines around an ogive-cylinder body and sectional side force coefficient along the body; $M_\infty = 0.2$, $\alpha = 30$ deg, and $Re_D = 3.0 \times 10^6$.

The role of the disturbance size and its effect on the flow asymmetry can be demonstrated by presenting the sectional side force coefficient distribution along the body alongside the off-surface streamlines that describe the vortical structure of the flow around the body. The sectional side force coefficient C_y is defined as follows:

$$C_y(x) = \frac{f_y(x)}{\frac{1}{2}\rho_\infty V_\infty^2 D} \tag{3}$$

where D is the diameter of the cylinder, and the sectional side force $f_y(x)$ is obtained through integration of the pressure as follows:

$$f_y(x) = \int_0^{2\pi} p(x, \phi)\sin(\phi) r \, d\phi \tag{4}$$

Figure 2 shows the computed off-surface streamlines around the body and the sectional side force coefficient along the body for the small asymmetry. Also presented in the figure are the experimental data. A good agreement is observed for the axial locations for which experimental data are available (Lamont's data[6] include pressure measurements for values of x/D between 0.0 and 6.0). Streamlines emanating from one side of the body are represented by black lines, whereas streamlines emanating from the other side are represented by gray lines. The structure of the streamlines on opposite sides of the body shows that the asymmetry level is very low. Furthermore, the vortical structure resembles the structure of a symmetric flow where the vortices run parallel to the body. This is well reflected in the sectional side force distribution. The asymmetry level remains very low up to $x/D \approx 3.0$, resulting in a symmetric-like structure of the lee side vortices and a virtually zero sectional side force throughout the ogive part of the body. The low sectional side force values along the cylindrical part of the body are the result of the small asymmetry in that region.

The results for the large asymmetry case are presented in Fig. 3. In this case, the nose asymmetry created by the bigger bump grows rapidly, resulting in an asymmetric vortical structure. The sectional side force coefficient behaves accordingly, departing from zero right from the apex, reaching a maximum of $C_y \approx 0.4$ at $x/D \approx 5.0$. This is where the primary vortex from the right side of the body starts to curve away from the body, diminishing its effect, whereas the primary vortex from the left side remains close to body at this region, thus becoming more dominant. The experimental data presented in the figure show good agreement with the computational results and follow a trend that supports the computational findings even though no experimental data are available for the region $6.0 < x/D < 10.5$.

Ogive Cylinder Flow at $\alpha = 40$ deg

Figure 4 contains a description of the vortical structure by way of the computed off-surface streamlines around the body and a comparison between the computational sectional side force coefficient

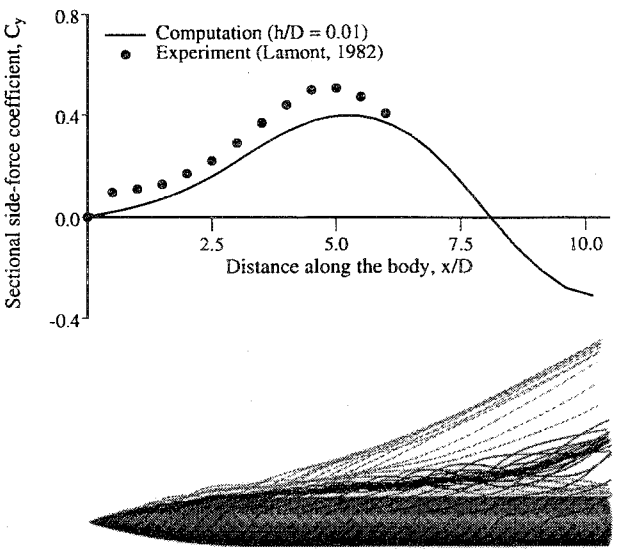

Fig. 3 Computed off-surface streamlines around an ogive-cylinder body and sectional side force coefficient along the body; $M_\infty = 0.2$, $\alpha = 30$ deg, and $Re_D = 4.0 \times 10^6$.

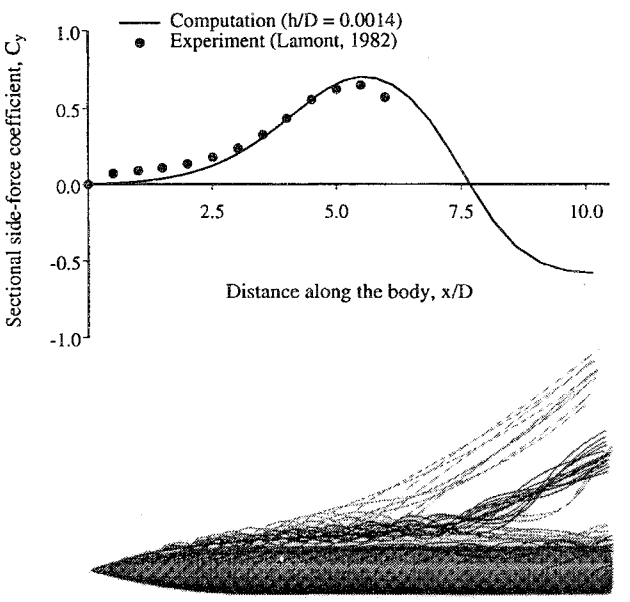

Fig. 4 Computed off-surface streamlines around an ogive-cylinder body and sectional side force coefficient along the body (the experimental results are reflected); $M_\infty = 0.28$, $\alpha = 40$ deg, and $Re_D = 3.0 \times 10^6$.

along the body and the experimental data. Just as for the two cases at $\alpha = 30$ deg, a good agreement between the computational and experimental results is observed. Note that the maximum value of sectional side force coefficient obtained here ($C_y \approx 0.5$) is roughly that obtained for the high-asymmetry-level case at $\alpha = 30$ deg (Fig. 3). However, the bump height required to produce it was only 14% of the height needed to simulate the high-asymmetry case at $\alpha = 30$ deg.

Results for this case further show the effect of the vortical structure on the sectional side force variation along the body. The primary vortex from the right side of the body curves away from the body at a point further upstream when compared with the large asymmetry case at $\alpha = 30$ deg. As a result, the primary vortex from the left side also curves away at a further upstream location, allowing the second vortex to develop and to create a suction peak that causes the crossing point of the sectional side force with zero to move further upstream as well. This is all the result of the higher sensitivity of the flow in this regime to surface imperfections. Although the asymmetry around the nose area is small, it grows to assume a fully developed asymmetric flow.

The simultaneous examination of the computed off-surface streamlines (Figs. 2–4) and the corresponding variation of the side force coefficient reveals that the results conform with the observations of Hunt and Dexter[4] and Dexter and Hunt[5] that the sectional side force is directed toward the side containing the vortex that lies closer to the body.

Systematic Study of the Effect of Bump Height Variation

Although, as observed, the results from the computational simulations were in good agreement with the experimental results of one roll angle position (Fig. 4), the achievement of a similar agreement for other roll angles might require changes in more than one parameter. Such changes might include the location of the disturbance, both axially and circumferentially, the introduction of additional disturbances, and changes to the disturbance geometry. The higher number of degrees of freedom will make the task of simulating the effect of an actual nose orientation a difficult one.

Rather than seek an appropriate bump height and location for each change in roll angle, in theory the problem could be solved simply by duplicating the exact geometry of the body, including the shape of minute imperfections at the tip, and an accurate representation of minute surface roughness elements. The computer simulation would then require sufficient grid resolution to achieve an accurate reproduction of the body geometry. In principle, achieving a perfect match between the numerically simulated model and the wind-tunnel model should allow computational results to match experimental data for every roll angle. This solution is currently infeasible owing to the high computational costs. However, it will be shown later that, at least qualitatively, the essential features of flow asymmetry can be captured by the use of a simple simulated disturbance. The numerical results presented in this section correspond to the flow conditions $M_\infty = 0.28$, angle of attack $\alpha = 40$ deg, Reynolds number $Re_D = 3.0 \times 10^6$, and bump heights between $h/D = 0.0008$ and 0.01. The available experimental data[6] included pressure measurements from seven different roll angle positions.

Figures 5–7 show the computed off-surface streamlines around the body and the sectional side force coefficient along the body for bump heights $h/D = 0.0008$, 0.002, and 0.01, respectively. These three cases represent the range of solutions that were obtained through systematic changes to bump height. The vortical structure of the small asymmetry case (Fig. 5) remains symmetric around the nose region and becomes asymmetric around the cylindrical part of the body. This is well reflected in the sectional side force coefficient distribution along the body. The side force coefficient remains virtually zero throughout the ogive part of the body, whereas the strength difference between the vortices around the cylindrical region is sufficient to create a sizable sectional side force toward the end of the body. The large asymmetry cases (Figs. 6 and 7) exhibit fully developed asymmetric vortical structures that are reflected in the sectional side force coefficient variation of the respective cases. Both show how the lengthwise-periodic distribution of the side force is a direct result of the lengthwise-periodic vortical structure. Further

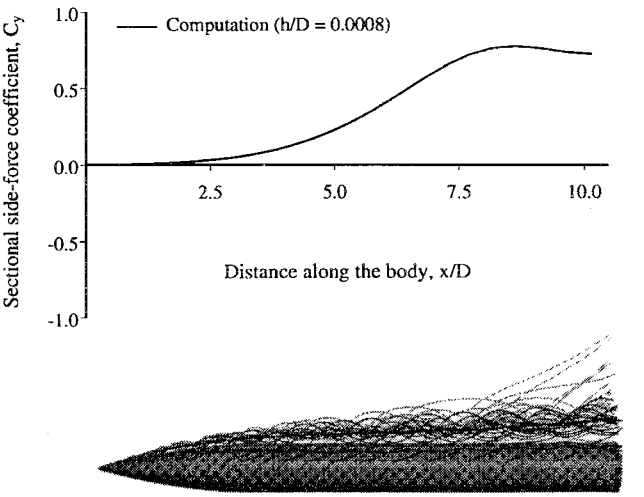

Fig. 5 Computed off-surface streamlines around an ogive-cylinder body and sectional side force coefficient along the body; $M_\infty = 0.28$, $\alpha = 40$ deg, and $Re_D = 3.0 \times 10^6$.

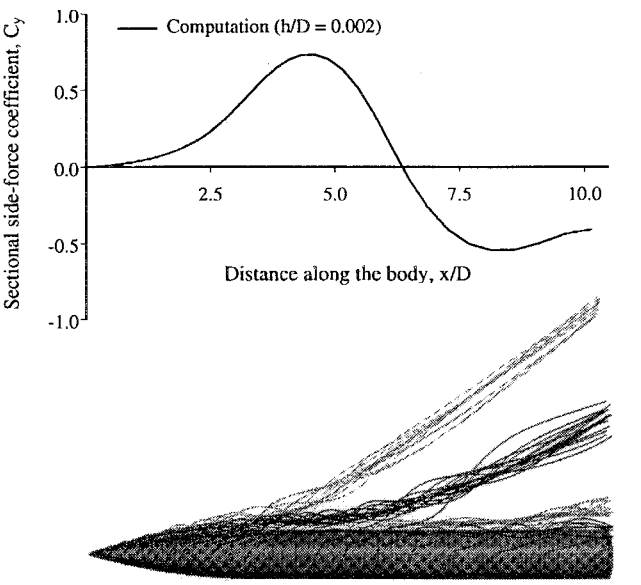

Fig. 6 Computed off-surface streamlines around an ogive-cylinder body and sectional side force coefficient along the body; $M_\infty = 0.28$, $\alpha = 40$ deg, and $Re_D = 3.0 \times 10^6$.

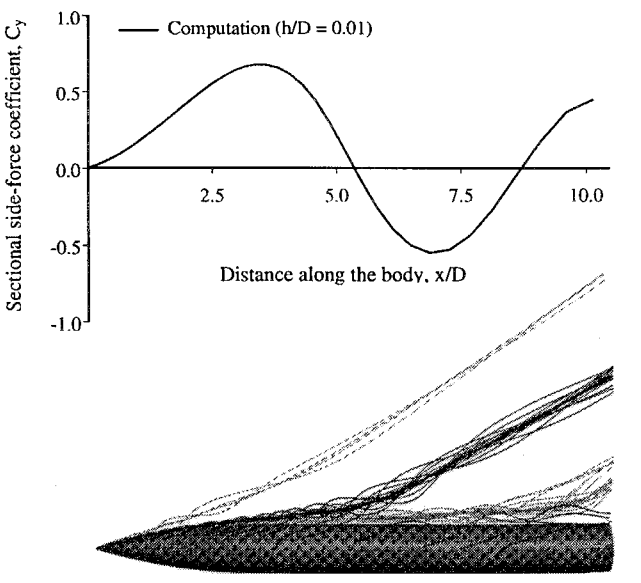

Fig. 7 Computed off-surface streamlines around an ogive-cylinder body and sectional side force coefficient along the body; $M_\infty = 0.28$, $\alpha = 40$ deg, and $Re_D = 3.0 \times 10^6$.

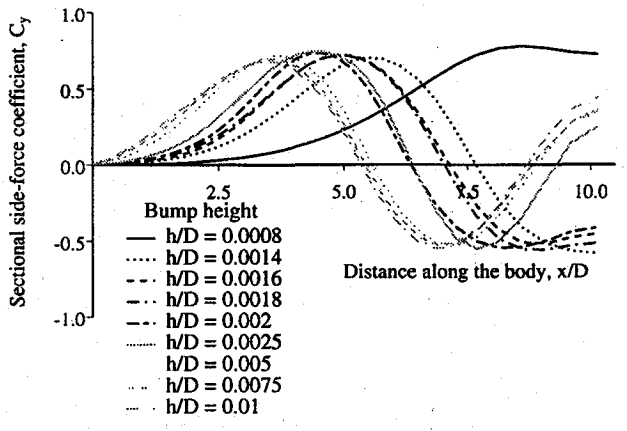

Fig. 8 Sectional side force coefficient for several bump sizes (computation); $M_\infty = 0.28$, $\alpha = 40$ deg, and $Re_D = 3.0 \times 10^6$.

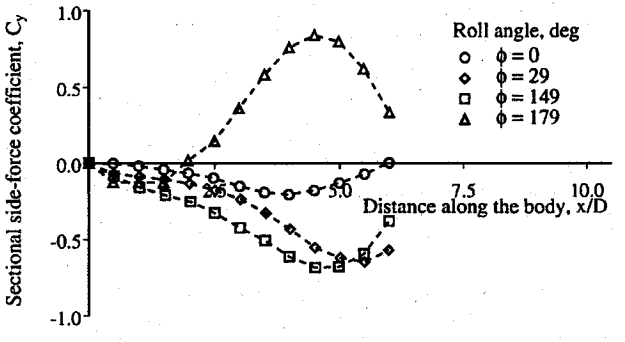

Fig. 9 Sectional side force coefficient for several roll angles (experiment, data extracted from Refs. 6 and 7); $M_\infty = 0.28$, $\alpha = 40$ deg, and $Re_D = 3.0 \times 10^6$.

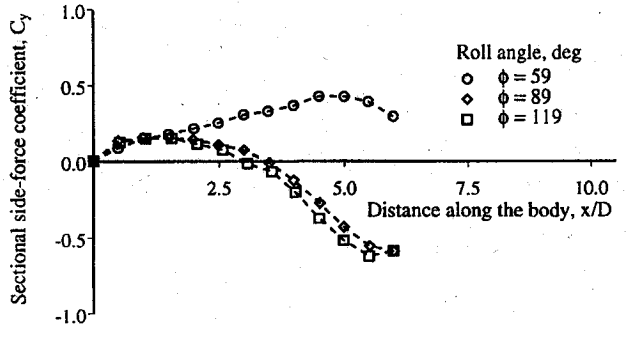

Fig. 10 Sectional side force coefficient for several roll angles (experiment, data extracted from Refs. 6 and 7); $M_\infty = 0.28$, $\alpha = 40$ deg, and $Re_D = 3.0 \times 10^6$.

examination of all four cases corresponding to these flow conditions (Figs. 4–7) show that there is an excellent correlation between the location where the vortices curve away from the body and the location of the maxima, minima, and zero crossing of the sectional side force coefficient.

Figure 8 shows the variation of the sectional side force coefficient along the body for the different bump height cases that were computed. It is assumed that the mirror image of each of these simulated cases could have been obtained by placing the bump on the opposite side of the symmetry plane. This assumption is based on the fact that the flux-split algorithm has symmetry-preserving properties and therefore is unbiased.[29,30]

The experimental results of the variation of sectional side force coefficient along the body for the different roll angle positions are divided into two figures. One, Fig. 9, includes results from four roll angle positions for which the sectional side force coefficient is negative near the body apex, and the other, Fig. 10, includes results from three roll angle positions for which the sectional side force coefficient near the body apex is positive.

Of all 18 bump heights for which results were obtained (the 9 cases that were actually computed plus 9 mirror images), only the computational results for bump height $h/D = 0.0014$ match the experimental data. The data correspond to the roll angle position of $\phi = 29$ deg (see Fig. 4). Although the other computed cases do not match any of the other roll angle position measurements, the computational and experimental results follow the same trends. For the computational results, the sectional side force variation along the body is almost uniquely determined by the bump height. Increasing the bump height from $h/D = 0.0008$ to 0.01 results in a consistent increase of the sectional side force level near the nose. The increase is caused by the higher asymmetry level in this region caused by the bump. A larger bump also causes the first primary vortex to curve away from the body at a point further upstream, creating a lower pressure area that allows the second primary vortex to curve away as well, this one from the other side of the body. This results in a lengthwise-periodic distribution of the sectional side force that alternates in sign. Increasing the bump height also causes the axial location where the sectional side force variation crosses zero to move upstream (see Fig. 8). Note that the maximum value of sectional side force coefficient tends to reach the same limit for all bump sizes. Further, when the bump is increased beyond a certain threshold, the axial distance between the maximum and minimum of the sectional side force coefficient remains almost constant. This is because the lengthwise distance between the primary vortices from opposite sides of the body remains virtually unchanged as well.

A similar evaluation of the experimental results requires an approximation of the disturbance level for each of the experimental results. The level of disturbance that is the net result of the nose imperfections is not known, but it is obvious from Figs. 9 and 10 that every roll angle position creates a different disturbance to the flow. One way of approximating the actual disturbance created at each of the various roll angle positions is to use the sectional side force coefficient at the closest point to the apex (at $x/D = 0.5$) as an indicator of the disturbance magnitude. Adopting this approximation permits the following observations. Although the data available from the experiment extend only to $x/D = 6.0$, one can see that the sectional side force variation along the body also will be lengthwise periodic. Just as for the computational results, a larger disturbance near the nose causes the axial location where the sectional side force coefficient crosses zero to move upstream.

Further analysis of the computational and experimental results reveals the effect of the disturbance on the total side force coefficient. One might expect that an increase of the disturbance would yield a higher overall side force coefficient, but the results show that this is not necessarily the case. For example, increasing the bump height from $h/D = 0.0008$ to 0.0014 causes the sectional side force along the body to pass through zero, resulting in a decrease of the total side force coefficient (see Fig. 11). An additional increase of the bump height results in a still smaller total side force. This trend changes when the bump height is increased from $h/D = 0.002$ to 0.0025, where an increase in the total side-force coefficient is observed. Further increase of the bump height results in a saturation of the side force coefficient. This behavior, that is consistent with

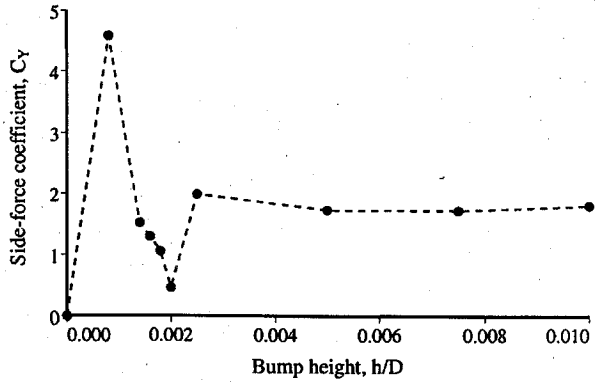

Fig. 11 Overall side force coefficient for various bump heights (computation); $M_\infty = 0.28$, $\alpha = 40$ deg, and $Re_D = 3.0 \times 10^6$.

experimental observations, suggests that different asymmetric flows may yield the same overall side force.

The experimental results exhibit similar trends. The nose orientation of the model at the roll angle of $\phi = 0$ deg is such that it creates a small perturbation resulting in a low side force coefficient, $C_Y = -0.77$. A larger perturbation was created by placing the model at a roll angle of $\phi = 29$ deg, resulting in a higher side force, $C_Y = -2.34$. Placing the model at the roll angle of $\phi = 179$ deg created an even larger disturbance, but the overall side force coefficient has become positive, $C_Y = 2.46$. These results indicate that the sign and magnitude of the side force coefficient cannot be used as an indication of the level of flow asymmetry. One must investigate the whole flowfield to determine the asymmetry level. Furthermore, both experimental and computational results presented in this section show that the asymmetric solutions change with every change in flow conditions. This observation supports the school of thought claiming that the flow asymmetry is the result of a convective instability mechanism.

Summary

The complex flow structure exhibited by high-angle-of-attack flow around the ogive cylinder body was simulated by using an unbiased flow solver, a perfectly symmetric computational mesh, and a disturbance appropriately placed near the body apex. This disturbance represents the small surface roughness that exists on wind-tunnel models. The qualitative comparison between the numerical results corresponding to different disturbance sizes and experimental results corresponding to different roll angle orientations revealed that the variation of the sectional side force coefficient along the body can be used to characterize asymmetric flows. The good correlation between the sectional side force variation along the body and the vortical structure indicate that the results of the numerical simulations are consistent with the observations made by Hunt and Dexter[4] and Dexter and Hunt.[5] It is also shown that the variation of the sectional side force around the body apex virtually determines its variation along the rest of the body.

The abilities to control the degree of asymmetric flow and to produce flows that depend continuously on the size of the disturbance support the hypothesis that this feature of the asymmetric flow is consistent with the presence of a convective instability mechanism. The experimental results corresponding to the seven different roll angle positions that were presented likewise showed that results changed as the roll angle position changed, thus providing additional experimental evidence in support of this hypothesis.

Acknowledgments

This work has been supported in part by NASA Grant NCA2-765 and National Science Foundation Grant ECS-9215145. The work of the third author was supported by the Israel Science Foundation administered by the Israel Academy of Sciences and Humanities.

References

[1]Hunt, B. L., "Asymmetric Vortex Forces and Wakes on Slender Bodies," AIAA Paper 82-1336, Aug. 1982.

[2]Ericsson, L. E., and Reding, J. P., "Asymmetric Vortex Shedding from Bodies of Revolution," Vol. 104, Progress in Astronautics and Aeronautics, AIAA, New York, 1986, pp. 243–296.

[3]Ericsson, L. E., and Reding, J. P., "Asymmetric Flow Separation and Vortex Shedding on Bodies of Revolution," *Tactical Missile Aerodynamics: General Topics*, edited by M. J. Hemsch, Vol. 141, Progress in Astronautics and Aeronautics, AIAA, Washington, DC, 1992, pp. 391–452.

[4]Hunt, B. L., and Dexter, P. C., "Pressures on a Slender Body at High Angle of Attack in a Very Low Turbulence Level Airstream," AGARD CP 247, Paper 17, 1978.

[5]Dexter, P. C., and Hunt, B. L., "The Effect of Roll Angle on the Flow over a Slender Body of Revolution at High Angles of Attack," AIAA Paper 81-0358, Jan. 1981.

[6]Lamont, P. J., "The Complex Asymmetric Flow over a 3.5D Ogive Nose and Cylindrical Afterbody at High Angles of Attack," AIAA Paper 82-0053, Jan. 1982.

[7]Lamont, P. J., "Pressures Around an Inclined Ogive Cylinder with Laminar, Transitional, or Turbulent Separation," *AIAA Journal*, Vol. 20, 1982, pp. 1492–1499.

[8]Zilliac, G. G., Degani, D., and Tobak, M., "Asymmetric Vortices on a Slender Body of Revolution," *AIAA Journal*, Vol. 29, 1991, pp. 667–675.

[9]Allen, H. J., and Perkins, E. W., "Characteristics of Flow over Inclined Bodies of Revolution," NACA RM A50L07, 1951.

[10]Allen, H. J., and Perkins, E. W., "A Study of Effect of Viscosity on Flow over Slender Inclined Bodies of Revolution," NACA Rept. 1048, 1951.

[11]Thomson, K. D., and Morrison, D. F., "The Spacing, Position and Strength of Vortices in the Wake of Slender Cylindrical Bodies at Large Incidence," *Journal of Fluid Mechanics*, Vol. 50, 1971, pp. 751–783.

[12]Degani, D., "Numerical Investigation of the Origin of Vortex Asymmetry," AIAA Paper 90-0593, Jan. 1990.

[13]Degani, D., "Effect of Geometrical Disturbance on Vortex Asymmetry," *AIAA Journal*, Vol. 29, 1991, pp. 560–566.

[14]Degani, D., and Schiff, L. B., "Numerical Simulation of the Effect of Spatial Disturbances on Vortex Asymmetry," *AIAA Journal*, Vol. 29, 1991, pp. 344–352.

[15]Siclari, M. J., and Marconi, F., "The Computation of Navier–Stokes Solutions Exhibiting Asymmetric Vortices," AIAA Paper 89-1817, June 1989.

[16]Kandil, O. A., Wong, T. C., and Liu, C. H., "Navier–Stokes Computations of Symmetric and Asymmetric Vortex Shedding Around Slender Bodies," AIAA Paper 89-3397, Aug. 1989.

[17]Degani, D., and Tobak, M., "Numerical, Experimental, and Theoretical Study of Convective Instability of Flows over Pointed Bodies at Incidence," AIAA Paper 91-0291, Jan. 1991.

[18]Degani, D., and Tobak, M., "Experimental Study of Controlled Tip Disturbance Effect on Flow Asymmetry," *Physics of Fluids A*, Vol. 4, Dec. 1992, pp. 2825–2832.

[19]Williams, D., and Bernhardt, J., "Proportional Control of Asymmetric Forebody Vortices with the Unsteady Bleed Technique," AIAA Paper 90-1629, June 1990.

[20]Degani, D., and Tobak, M., "Effect of Upstream Disturbance on Flow Asymmetry," AIAA Paper 92-0408, Jan. 1992.

[21]Degani, D., and Levy, Y., "Asymmetric Turbulent Vortical Flows over Slender Bodies," *AIAA Journal*, Vol. 30, 1992, pp. 2267–2273.

[22]Baldwin, B. S., and Lomax, H., "Thin Layer Approximation and Algebraic Model for Separated Turbulent Flows," AIAA Paper 78-257, Jan. 1978.

[23]Steger, J. L., "Implicit Finite-Difference Simulation of Flow About Arbitrary Two-Dimensional Geometries," *AIAA Journal*, Vol. 16, 1978, pp. 679–686.

[24]Steger, J. L., Ying, S. X., and Schiff, L. B., "A Partially Flux-Split Algorithm for Numerical Simulation of Unsteady Viscous Flows," Workshop on Computational Fluid Dynamics, Univ. of California, Davis, CA, June 1986.

[25]Ying, S. X., Baganoff, D., Steger, J. L., and Schiff, L. B., "Numerical Simulation of Unsteady, Viscous, High-Angle-of-Attack Flows Using a Partially Flux-Split Algorithm," AIAA Paper 86-2179, Aug. 1986.

[26]Cebeci, T., Smith, A. M. O., and Mosinkis, G., "Calculation of Compressible Adiabatic Turbulent Boundary Layers," *AIAA Journal*, Vol. 8, 1970, pp. 1974–1982.

[27]Degani, D., and Schiff, L. B., "Computation of Turbulent Supersonic Flows Around Pointed Bodies Having Crossflow Separation," *Journal of Computational Physics*, Vol. 66, 1986, pp. 173–196.

[28]Degani, D., Schiff, L. B., and Levy, Y., "Numerical Prediction of Subsonic Turbulent Flows over Slender Bodies at High Incidence," *AIAA Journal*, Vol. 29, 1991, pp. 2054–2061.

[29]Levy, Y., "Numerical Analysis of Three-Dimensional Flow Solvers Applied to High-Angle-of-Attack Flows," Ph.D. Thesis, Aeronautics and Astronautics Dept., Stanford Univ., Stanford, CA, 1994.

[30]Levy, Y., Hesselink, L., and Degani, D., "Anomalous Asymmetries in Flows Generated by Algorithms that Fail to Conserve Symmetry," AIAA Paper 94-2287, June 1994.